Pergamon

0042-6989(95)00327-4

Vision Res., Vol. 36, No. 16, pp. 2609–2621, 1996

Printed in Great Britain
0042-6989/96 $15.00 + 0.00

An Alternative Phototransduction Model for Human Rod and Cone ERG *a*-waves: Normal Parameters and Variation with Age

ARTUR V. CIDECIYAN,*†‡ SAMUEL G. JACOBSON*†‡

Received 25 January 1995; in revised form 20 June 1995; in final form 1 December 1995

A quantitative description of the activation reactions in the cGMP phototransduction cascade has been recently developed [Lamb & Pugh (1992). *Journal of Physiology, 449*, 719–758]. When applied to the human electroretinogram *a*-wave, the widely used simplified form of this model provides a good description of all waveforms except those elicited with very high energy stimuli. The basis for these misfits at high energies is explored in the current study and an alternative model of phototransduction is derived that retains the quantitative aspects but avoids certain simplifying assumptions previously made. The new model describes well both rod- and cone-isolated *a*-waves over a large range of stimulus energies extending up to those that cause significant bleaching. To facilitate clinical application of this methodology, a short test protocol is developed and normal data for rod and cone transduction parameters are provided over a wide age range. In the sample of normal subjects studied, maximum amplitude of rod and cone *a*-waves and sensitivity of the cone *a*-wave do not change with age. An age-related decline in rod *a*-wave sensitivity is present and it is greater than that expected from pre-retinal absorption alone. Copyright © 1996 Elsevier Science Ltd.

cGMP phototransduction cascade | Computational modeling | Electroretinogram (ERG) *a*-wave | Human rod and cone photoreceptors

INTRODUCTION

For more than 50 years, the electroretinogram (ERG) *a*-wave has been considered to originate from the photoreceptors (Granit, 1933; Penn & Hagins, 1969) but only recently has the exact relationship between this waveform and the underlying biochemistry of phototransduction become more clearly understood. The first advance came when the leading edge of the human rod-isolated ERG *a*-wave was shown (Hood & Birch, 1990) to be well described by the same mathematical model that was used to describe the light-evoked blockage of current flow in suction electrode recordings of primate rod receptors (Baylor *et al.*, 1984). Further progress occurred when analysis of the activation steps of the cGMP phototransduction cascade theory led to the formulation of a mathematical model that accounts quantitatively for the kinetics and amplification of the rising phase of the rod photocurrent (Lamb & Pugh, 1992; Pugh & Lamb, 1993). Using several simplifying assumptions, this model predicts the photocurrent to rise as a delayed Gaussian function of time. Stochastic simulation of the two dimensional diffusional interactions that occur at the rod disc membrane confirmed the main predictions of this model (Lamb, 1994).

The mathematical simplicity and direct biochemical relevance of the delayed Gaussian approximation of the phototransduction model led to its prompt acceptance as a potentially valuable means to study human photoreceptor function. It has already been applied to the analysis of the leading edges of ERG *a*-waves recorded from normal subjects (Pugh & Lamb, 1993; Hood & Birch, 1993a) and from patients with retinal disease (for example Cideciyan & Jacobson, 1993; Breton *et al.*, 1994; Jacobson *et al.*, 1994; Hood & Birch, 1994; Hood *et al.*, 1995). Our experience in the use of this simplified model for analyses of normal and abnormal human ERG *a*-waves led to the observation that although the model fits well to waveforms under certain conditions, there are definite problems with the fits to *a*-waves evoked with higher energy stimuli. Two hypotheses can be offered to explain these misfits at high energies. First, they could be the result of the failure of biochemical assumptions underlying the model. The second and simpler hypothesis

*To whom all correspondence should be addressed in Philadelphia.
†Bascom Palmer Eye Institute, University of Miami School of Medicine, 1638 NW 10th Avenue, Miami, FL 33136, U.S.A.
‡Scheie Eye Institute, University of Pennsylvania, 51 North 39th Street, Philadelphia, PA 19104, U.S.A.

is that the validity of the technical assumptions made to derive the delayed Gaussian approximation of the model need to be reconsidered at high energies.

We examined the second hypothesis and derived an alternative version of the phototransduction model which specifically allows for a finite stimulus time course, three cascaded first-order delay stages, and the capacitive time constant of the photoreceptor membrane. The new version of the model fits families of rod-isolated responses better than the delayed Gaussian approximation. In the present study, we describe our alternative version of the phototransduction model and compare it with the delayed Gaussian approximation in the analysis of human rod ERG *a*-waves. In addition to providing better fits of the rod waveforms, the alternative model also describes cone-isolated ERG *a*-waves, thereby allowing direct comparison of rod and cone phototransduction parameters. Responses to high energy stimuli that isomerize up to 2.5% of the pigment in rods and up to 1% in cones are fitted well by the newer model. In anticipation of more widespread clinical use of *a*-wave recording and modeling, we examine the reliability of the model in analysis of results from shortened protocols and also report normal limits for rod and cone transduction parameters and their variation with age.

METHODS

Subjects

The 17 subjects in this study had normal eye examinations. The age range was 18–75 yr; there were nine men and eight women. The same eye of 14 subjects was used for rod-isolated and cone-isolated ERG *a*-wave recordings; the tests were performed on different days. Two subjects underwent only cone-isolated *a*-wave recordings and one subject had *a*-wave recordings to bright white flashes only. The procedures were in accordance with institutional guidelines and each subject gave written consent after the nature and potential risks of the recordings were explained.

Recording technique

Full-field ERGs were performed using unipolar Burian–Allen contact lens electrodes (Hansen Ophthalmics, Iowa City, IA), a custom-built ganzfeld, and a computer-based recording system (Pathfinder II, Nicolet Instruments Corp., Madison, WI). The contact lens electrode was referenced to an indifferent forehead electrode that was protected from light exposure; the ground electrode was located at the ear lobe. The signals were amplified (band-pass 0.5–1000 Hz; 4-pole) and digitized with an 8-bit analog-to-digital converter over a 2 mV peak-to-peak dynamic range at a 2.5 kHz sampling rate for a duration of 200 msec (Cideciyan & Jacobson, 1993). The stimulus was produced by a helical Xenon flash tube (MW8QV; 900 V, 3200 J; Speedotron Corp., Chicago, IL) coupled from above to the ganzfeld with intervening IR blocking filter and two movable filter trays carrying gelatin (Wratten; Eastman Kodak Co., Rochester, NY) colored and neutral density filter combinations. The flash tube was driven with a power supply (2401B; Speedotron Corp., Chicago, IL) capable of delivering 2400 J per flash with a maximum repetition rate of 0.3 Hz. Flash to flash energy variability was < 5% with a semi-random inter-flash interval. In order to minimize the flash duration, reduced energy (400 J; unattenuated white ganzfeld luminance = 2300 cd sec m^{-2}) was applied to the flash tube.

Rod-isolated ERGs were derived computationally from families of responses to different energies of blue (Wratten 47A; λ_{max} = 440 nm band-pass) and red (Wratten 26; $\lambda_{50\%}$ = 605 nm long-pass) flashes delivered in a dark-adapted state. The energies were selected to provide pairs of scotopically matched responses to blue and red flashes, which, when digitally subtracted gave a dark-adapted cone ERG, that was then subtracted from the response to a blue flash photopically matched to the red flash (Sandberg *et al.*, 1990; Cideciyan & Jacobson, 1993). It has been recently shown that removal of the cone component from bright flashes may be important for accurate estimation of rod transduction parameters (Hood & Birch, 1994). Responses to a pair of flashes were averaged for stimuli up to 2 log scot td sec and single flash responses were used in brighter stimuli. The subjects were dark adapted for 45 min; complete mydriasis was achieved with tropicamide (1%) and phenylephrine hydrochloride (10%). Scotopically, the brightest blue stimulus used was 4.6 log scot td sec (8 mm pupil). The interstimulus interval was increased with energy and it ranged from 10 sec at low energies to several minutes at the highest energies.

"Mixed" rod and cone high energy *a*-waves were recorded with white stimuli in a dark-adapted state in one normal subject. The brightest stimulus was 5.4 log scot td sec, which corresponded to 5.1 log phot td sec. The rod receptor component of each mixed response was calculated by subtracting the model-based extrapolated estimate of the cone receptor contribution at the corresponding photopic energy. The cone model parameters were determined from lower energy dark-adapted cone-isolated responses derived using scotopically matched red and blue stimuli in the same subject.

Cone-isolated high energy *a*-waves were recorded with red (Wratten 26) stimuli on a white background (30 cd m^{-2}). This adapting field does not significantly affect the sensitivity of the cone *a*-wave, but it is sufficient to remove the rod contribution to bright red flashes (Hood & Birch, 1993b). Four to 16 responses, recorded with an interstimulus interval of 3 sec, were averaged. Photopically, the brightest red stimulus was 4.1 log phot td sec.

Mathematical analysis

All mathematical modeling was performed using Matlab (Version 4.2; The MathWorks, Inc, Natick, MA) running on an IBM/PC compatible computer. Models were fitted to the leading edge of the rod- and cone-isolated ERG *a*-waves by minimizing the average root-mean-squared (r.m.s.) error using a simplex algo-

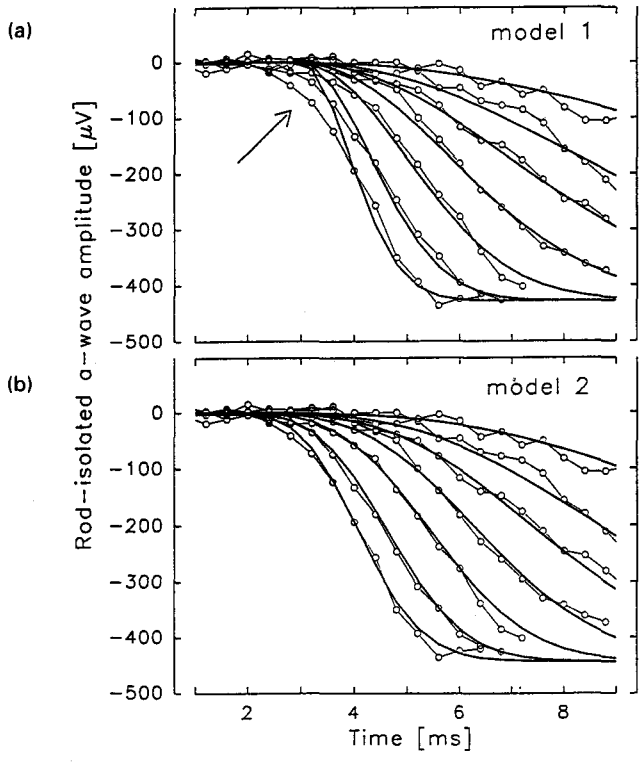

FIGURE 1. Comparison of two models of phototransduction (thick lines) fitted to the leading edges of rod-isolated ERG *a*-wave data (symbols and thin lines) from a representative normal subject. (a) Shows model 1 and (b) shows model 2. The family of responses are to 2.6, 3.1, 3.3, 3.6, 3.9, 4.3, and 4.6 log scot td sec stimuli. For the ERGs of this normal subject, the parameters determined by ensemble fitting are R_{max} = 428 μV, σ = 1.48 log scot td^{-1} sec^{-3}, and t_{eff} = 2.98 msec for model 1, and R_{max} = 443 μV, σ_{sc} = 1.59 log scot td^{-1} sec^{-3}, and τ_{sc} = 0.75 msec for model 2. At high stimulus energies, model 1 misfits the data (arrow) whereas model 2 does not.

rithm (Nelder & Mead, 1965). The average r.m.s. error was defined as the average of r.m.s. errors calculated individually for each waveform in a series. This approach gave equal "weight" to each response; otherwise, responses to higher energy stimuli, having smaller number of samples due to the earlier *b*-wave intrusion, would have received less "weight" than those to lower energy stimuli. Some of the model parameters were iterated through a logarithmic transformation in order to limit their range to positive numbers. The convolutions were performed using a 0.05 msec sampling interval.

The end of the leading edge of a rod *a*-wave was defined by the point of *b*-wave intrusion or 15 msec, whichever came first. For the highest energy stimulus response, *b*-wave intrusion was defined as the point where the waveform becomes more positive. For all other responses, *b*-wave intrusion was defined as the sample that precedes the *a*-wave trough. The end of the leading edge of the cone *a*-wave was defined similarly by the sample that precedes the first oscillatory potential or 12 msec, whichever came first. The noise level of each waveform was quantified by calculating the standard deviation of the data over a 19 msec time span preceding the stimulus. The average value of the prestimulus baseline was used to equate the zero-potential for waveforms in a family.

RESULTS

Rod phototransduction model

Figure 1 shows the leading edge of a rod-isolated ERG *a*-wave series from a normal subject (symbols and thin lines) fitted by two models of rod phototransduction. "Model 1" [Fig. 1(a)] refers to the delayed Gaussian model of receptor photocurrent [equation (6.10); Lamb & Pugh, 1992] which is scaled and inverted in order to be applicable to corneally recorded rod-isolated ERG *a*-wave potentials:

$$R(I_{sc}, t) = R_{max}\left[1 - \exp\left(-\frac{1}{2} I_{sc}\,\sigma_{sc}\,(t - t_{eff})^2\right)\right] \quad \text{for } t \gg t_{eff} \tag{1}$$

where $R(I_{sc},t)$ is the corneally measured potential in μV; I_{sc}, the retinal illuminance of the stimulus in scot td sec; t, the time after stimulus onset in seconds; R_{max}, the maximum response amplitude in μV; σ_{sc}, the sensitivity of the response in scot td^{-1} sec^{-3}; and t_{eff}, a brief time delay in seconds. With model 1, normal parameter statistics (mean $\pm$ SD) were as follows: R_{max} = 441 $\pm$ 52 μV, σ_{sc} = 1.41 $\pm$ 0.14 log scot td^{-1} sec^{-3}, and t_{eff} = 3.14 $\pm$ 0.17 msec. The average r.m.s. error was 18.6 $\pm$ 3.0 μV.

Careful examination of the fit of model 1 to the data reveals that at high stimulus energies the model and the waveforms are behaving very differently (Fig. 1, arrow). Specifically, the model describes families of waveforms with a constant latency and an increasing slope. In contrast, with higher stimulus energies, the ERG *a*-waves attain a constant slope and a shortening latency. This was a consistent finding in all subjects studied by us; others have also reported similar behavior of the human (Breton *et al.*, 1994) and rat (Findl *et al.*, 1995) ERG *a*-waves. Although the misfits at high energies may be due to the failure of biochemical assumptions, a simpler and more parsimonious explanation may be provided by reconsideration of the validity of the technical assumptions made to derive model 1.

It has been assumed for example, that both the stimulus duration and the biochemical reaction delays are brief relative to the times of the electrical responses involved. Furthermore, the capacitive time constant of the rod photoreceptor membrane is assumed to be negligible. These assumptions are not always applicable to rod-isolated ERG *a*-waves. The high energy flash stimuli used by us and others have a finite and significant duration relative to the latency of the ERG *a*-waves they evoke. Furthermore, the effects of biochemical reaction delays and the capacitive time constant of the receptor membrane are not negligible relative to the very high rate of rise of the evoked *a*-waves. Therefore, we have derived (see Appendix) an alternative phototransduction

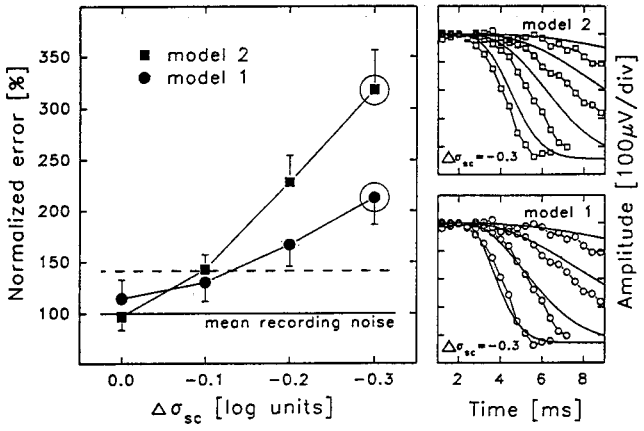

FIGURE 2. Left panel is a plot of error vs forced variation of the sensitivity parameter from its optimal value. Errors are normalized by the mean recording noise of 16.2 μV (solid horizontal line); horizontal dashed line is mean recording noise plus two standard deviations. The minimum error for each model ($\Delta\sigma_{sc}$ = 0.0 log units) is determined by allowing all three model parameters to vary freely while fitting the ensemble of waveforms. The errors for sub-optimal parameters were calculated by fixing R_{max} to the optimal value, holding sensitivity invariant at 0.1, 0.2, or 0.3 log units below the optimal value, and allowing the time delay parameter (t_{eff} or τ_{sc}, depending on the model) to vary freely. Error bars on symbols represent 2 SD. Right panels are examples of the nonoptimal fits at a 0.3 log unit reduced sensitivity (large circles on symbols in left panel) with the two models using subsets of the data shown in Fig. 1.

model that specifically allows for the stimulus time course, impulse response of three cascaded biochemical reactions, and low-pass filtering due to cell membrane capacitance. Otherwise, our model follows all of the quantitative biochemical steps originally set forth by Lamb and Pugh (1992). Our alternative model is defined as:

$$R(I_{sc},t) = R_{max}\left[1-\exp\left(-\frac{1}{2}I_{sc}\sigma_{sc}\left\{(\epsilon^2-6\epsilon\tau_{sc}+12\tau_{sc}^2)-e^{-\frac{\epsilon}{\tau_{sc}}}(\epsilon^2+6\epsilon\tau_{sc}+12\tau_{sc}^2)\right\}\right)\right]\star e^{-\frac{\epsilon}{\tau_{rm}}} \quad (2)$$

where in addition to the parameters defined for model 1, τ_{sc} is the time constant, in seconds, of a cascade of three first order decays presumed to correspond to three dominant rod photoactivation reactions (see Appendix); $\epsilon = t - \delta$;, the time in seconds delayed by an incremental amount δ due to finite flash duration and system specific time delays (see Appendix); τ_{rm}, the capacitive time constant of the rod photoreceptor membrane in seconds; and $\star$ represents the convolution operation. Equation (2) will be referred to as "model 2". Note that for times long compared to the time constants, both models 1 and 2 have the same Gaussian form: $1-\exp(-kt^2)$.

Figure 1(b) shows the fit of model 2 (thick lines) to the same data as in (a). With model 2, normal parameter statistics (mean $\pm$ SD) were as follows: R_{max} = 456 $\pm$ 54 μV, σ_{sc} = 1.52 $\pm$ 0.15 log scot td^{-1} sec^{-3}, and τ_{sc} = 0.85 $\pm$ 0.10 msec. The constants δ and τ_{rm} were held invariant at 1.1 and 0.5 msec, respectively (see Appendix). It may be noted that the variation on the τ_{sc} parameter (SD = 0.10 msec) is small compared to the sampling interval of the data (0.40 msec). Refit of model 2 to responses from all normal subjects by holding τ_{sc} constant at 0.85 msec and allowing only R_{max} and σ_{sc} to vary, produced results that were identical by inspection to those where τ_{sc} was allowed to vary. The statistics of R_{max} and σ_{sc} did not change, the average r.m.s. error increased from 15.8 $\pm$ 2.3 μV to 16.2 $\pm$ 2.2 μV.

As is evident in Fig. 1, model 2 fits the leading edge of rod-isolated ERG *a*-wave families better than model 1. Specifically, model 2 describes families of waveforms with a saturated rate of rise at high energies. A further advantage of model 2 is that parameter values can be determined with greater accuracy than with model 1. Figure 2 (left) compares the increase in error between each model and data as a function of forced change in the sensitivity parameter. The minimum error for each model ($\Delta\sigma_{sc}$ = 0.0) corresponds to the optimal fit which is determined for the ensemble of waveforms by allowing three model parameters (R_{max}, σ_{sc}, and t_{eff} for model 1, τ_{sc} for model 2) to vary freely. The error values for sub-optimal parameters were calculated by holding response amplitude (R_{max}) constant at its optimal value, forcing reduced sensitivity and allowing the time delay parameter (t_{eff} or τ_{sc}) to vary in order to minimize the error.

Figure 2 (left panel) illustrates the following three points:

1. The optimal fit by either model produces an average r.m.s. error that is within the recording noise level;
2. The optimal fit by model 1 consistently produces more error than the fit by model 2; and
3. The suboptimal fits produce significantly larger errors with model 2 compared to model 1.

The last point is exemplified in Fig. 2 (right panels) where the same waveforms as in Fig. 1 are shown with the fits of the two models when sensitivity is 0.3 log units reduced from its optimal value. In the case of model 2, varying the effective time constant of activation (τ_{sc}) cannot compensate for the change in sensitivity and the model dramatically misfits the data. With model 1, however, the time delay parameter (t_{eff}) partially compensates for the forced change in sensitivity and the resulting fit has much less error. Thus, due to the interdependence of sensitivity (σ_{sc}) and time delay (t_{eff}), the parameters of model 1 have greater uncertainty associated with them.

The value of model 2 in analysis of human rod *a*-wave recordings was further tested by determining whether a reliable estimate of phototransduction parameters could be obtained with a reduced number of recorded responses. If fewer waveforms were required to obtain transduction parameters, the length of the testing protocol could be shortened, thereby facilitating implementation of *a*-wave recordings in clinical settings. Figure 3 shows the covariance of R_{max} and σ_{sc} parameters determined from a six-wave family of responses and those from a two-wave subset of the same family of waveforms (τ_{sc} held constant at 0.85 msec). The correlation coefficients

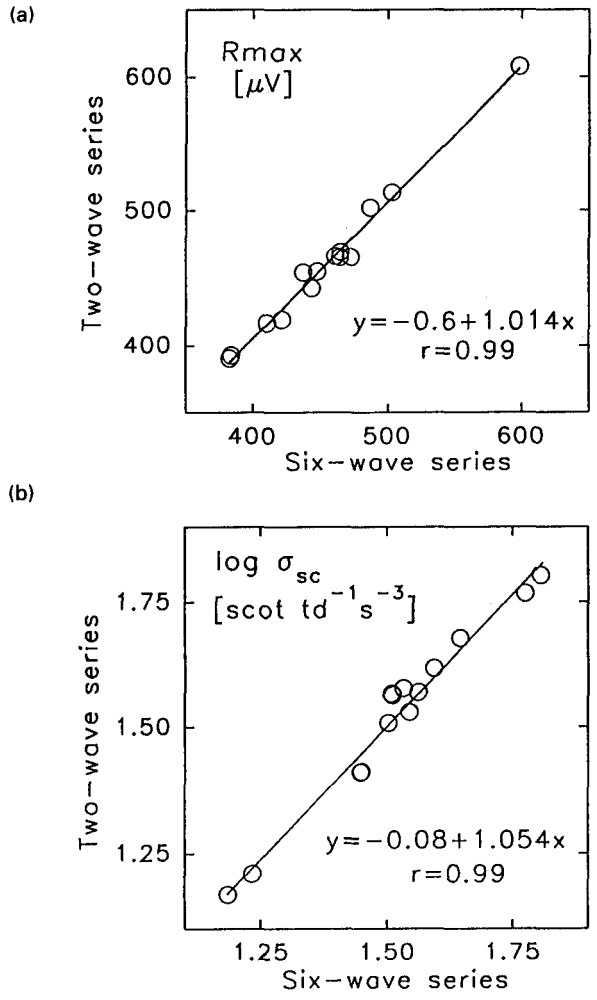

FIGURE 3. The maximum amplitude [R_{max}; (a)] and sensitivity [σ_{sc}; (b)] parameters of model 2 calculated using a six-wave (2.3, 2.6, 3.1, 3.3, 3.9, and 4.6 log scot td sec) rod-isolated ERG. *a*-waves are compared to those using only a two-wave subset (2.3 and 4.6 log scot td sec) of the same family. The resulting correlation coefficients and the linear regression parameters are also shown.

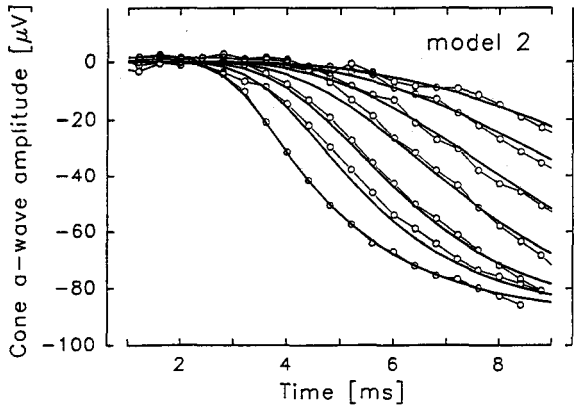

FIGURE 4. The leading edge of cone-isolated ERG *a*-waves of a representative normal subject (symbols and thin lines) fitted by the cone version of model 2 (thick lines). The family of responses are to stimuli in the range of 2.2–4.1 log phot td sec. The parameters for this normal subject determined by ensemble fitting are $R_{max} = 91.6\ \mu V$, $\sigma_{ph} = 2.31$ log phot td^{-1} s^{-3}, and $\tau_{ph} = 0.63$ msec.

are 0.99 and 0.99, and the resulting linear regression lines have slopes of 1.014 and 1.054, and *y*-intercepts of −0.6 and −0.08, for R_{max} and log σ_{sc}, respectively. For R_{max} and log σ_{sc} parameters the slopes are nearly one, and *y*-intercepts are nearly zero, thereby suggesting that the two-wave family is sufficient for the accurate determination of the rod phototransduction parameters using model 2.

Cone phototransduction model

Based on similarities in rod and cone transduction machinery, it would be expected that model 2 could also fit the leading edges of cone-isolated ERG *a*-waves to bright flashes. The time constants of activation and membrane capacitance would, of course, have to be changed to reflect the physiological and morphological differences between rods and cones (Pugh & Lamb, 1993). Thus, we define the cone version of model 2 similar to Eq. (2) where the parameters I_{sc}, σ_{sc}, τ_{sc}, τ_{rm} are replaced with I_{ph}, σ_{ph}, τ_{ph}, and τ_{cm}, respectively.*

Figure 4 shows cone-isolated *a*-waves (symbols and thin lines) from a normal subject; the cone version of model 2 is superimposed (thick lines). The normal parameter statistics (mean ± SD) were as follows: $R_{max} = 82.7 \pm 8.2\ \mu V$, $\sigma_{ph} = 2.28 \pm 0.14$ log phot td^{-1} sec^{-3}, and $\tau_{ph} = 0.44 \pm 0.09$ msec. The constant, δ, was the same as that used for rods (1.1 msec), and τ_{cm} was set equal to 2.0 msec. Similar to the rod-isolated *a*-wave parameters, it was observed that the effective time constant of cone activation (τ_{ph}) had very small variation. Holding τ_{ph} constant at 0.45 msec and allowing only R_{max} and σ_{ph} to vary did not change the statistics; the average r.m.s. error increased from 3.1 ± 0.9 μV to 3.2 ± 0.8 μV. The data suggest that the leading edge of the light-adapted cone *a*-wave is well characterized by the cone version of model 2.

Rod phototransduction with high energy stimuli

A dramatic reduction in sensitivity of the human rod *a*-wave at high stimulus energies has been described using model 1 (Breton *et al.*, 1994). It is important to know whether this is physiological or can be explained by the breakdown of technical assumptions made during simplification of the model. For this purpose, dark-adapted white stimulus ERG *a*-wave series extending from 2.2 to 5.4 log scot td sec were recorded from a normal subject; a lower energy red and blue stimulus series was also recorded. The cone component in the red series was estimated by subtracting scotopically matched blue responses. The cone version of model 2 was fitted to the estimated cone components and the ensemble best fit parameters were determined ($R_{max} = 70\ \mu V$, $\sigma_{ph} = 2.3$ log phot td^{-1} sec^{-3}; τ_{ph}, τ_{cm}, and δ held constant as before). The rod component of the responses to white

*sc = scotopic, ph = photopic, rm = rod membrane, cm = cone membrane.

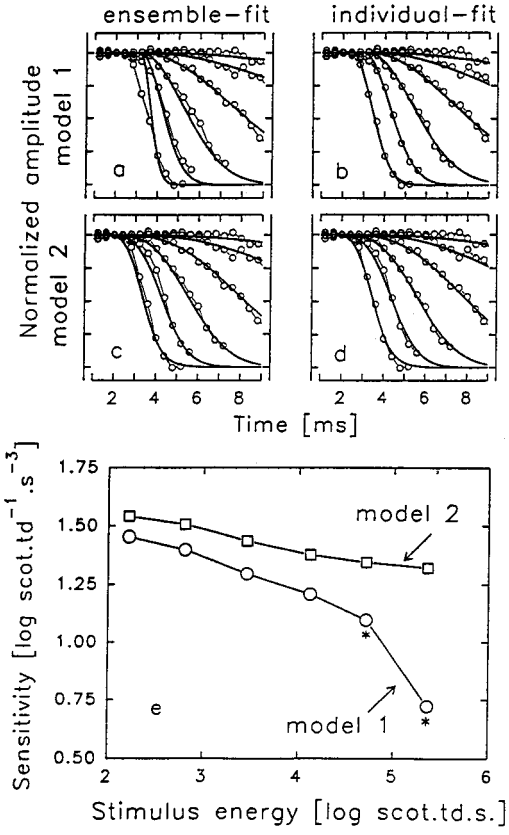

FIGURE 5. The fit of the two models [solid thick lines in (a)–(d)] to high energy ERG *a*-wave responses [symbols and thin lines in (a)–(d)] elicited by 2.2, 2.8, 3.5, 4.1, 4.7, and 5.4 log scot td sec stimuli. Maximum amplitude (R_{max}) parameter held invariant for all fits. (a) Ensemble fit using model 1. (b) Individual fits using model 1. (c) Ensemble fit using model 2. (d) Individual fits using model 2. (e) The sensitivity parameter (σ_{sc}) determined by fitting the two models individually to each waveform; for model 1, t_{eff} held invariant at mean normal value for all responses except those elicited by the two highest stimulus energies (marked with *); for model 2, τ_{sc} held invariant at mean normal value for all responses.

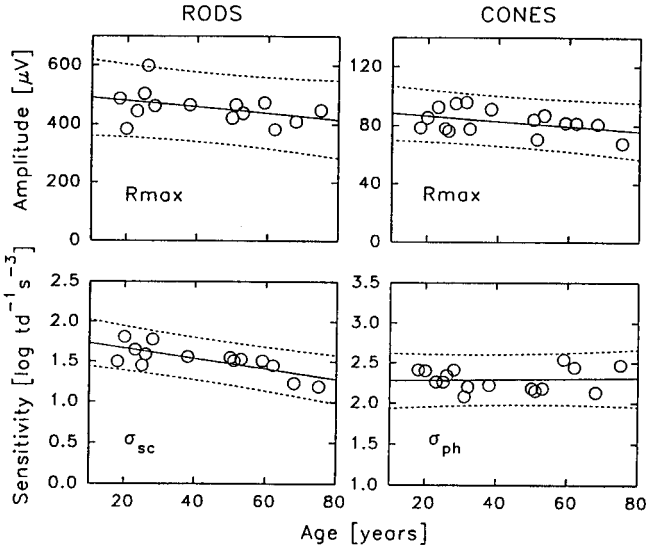

FIGURE 6. Maximum amplitude (R_{max}) and sensitivity (σ_{sc} or σ_{ph}) parameters of the rod and cone versions of model 2 plotted as a function of age. Ensemble fits to six-wave families were used for rods and seven-wave families for cones. The time constant of photoactivation was held invariant at 0.85 msec for rods and 0.45 msec for cones. Solid lines show regression lines, and dashed lines delimit the 95% prediction interval. Rod sensitivities (σ_{sc}) are in scot td^{-1} sec^{-3} units and cone sensitivities (σ_{ph}) are in phot td^{-1} sec^{-3} units.

stimuli was, in turn, estimated by subtracting the extrapolated cone model calculated at the photopic energies corresponding to each white flash. Figure 5 shows the presumed rod-isolated high energy data [symbols connected with thin lines, (a)–(d)], ensemble and individual fits by the models 1 [thick solid lines; (a) and (b)] and 2 [thick solid lines; (c) and (d)].

The R_{max} parameter was determined from the maximal response and was not varied for any of the fits. Figure 5(a) and (c) show the ensemble fits of model 1 (σ_{sc} = 1.27 log scot td^{-1} sec^{-3}; t_{eff} held constant at 3.14 msec) and model 2 (σ_{sc} = 1.40 log scot td^{-1} sec^{-3}; τ_{sc} held constant at 0.85 msec), respectively. Both models describe the lower energy responses equally well; as expected, model 1 fails to describe the highest energy responses whereas model 2 has no difficulty. Figure 5(b) and (d) show the individual fits of model 1 and model 2, respectively. Model 1 (b) was fitted by holding t_{eff} parameter constant at the mean normal value (3.14 msec) for energies up to 4.0 log scot td sec and allowing σ_{sc} parameter to vary for each waveform. For energies above 4.0 log scot td sec, both t_{eff} and σ parameters were allowed to vary in order to get fits that described the waveforms. Model 2 (d) was fitted to each individual waveform by allowing σ_{sc} to vary; τ_{sc}, τ_{rm}, and δ were held constant at their respective mean normal values. Clearly, both models describe equally well the complete range of responses as long as model parameters are allowed to vary individually for each waveform. However, it is important to point out that with model 1, considerable shortening of the time delay parameter is required at high energies (3.14, 2.95, and 2.43 msec at 4.1, 4.7, and 5.4 log scot td sec, respectively); this is not the case with model 2 which was fitted to all waveforms by holding the time constant of activation constant at the mean normal value.

Figure 5(e) plots the sensitivity parameter determined individually for each waveform in the series using the two models. For responses to stimuli from 2 to 4 log scot td sec, both models show a small reduction of sensitivity: 0.24 log units for model 1 and 0.16 log units for model 2. At higher stimulus energies, however, the two models differ considerably: from 4 to 5.4 log scot td sec model 1 shows 0.49 log units of reduction whereas model 2 shows only 0.06 log units. These results suggest that the dramatic reduction in sensitivity seen with model 1 at high energies may be an artefact of the failure of approximating the impulse response of a cascade of delay stages with a pure time delay.

Normal variation of rod and cone transduction parameters

Figure 6 shows the maximum amplitude and sensitivity

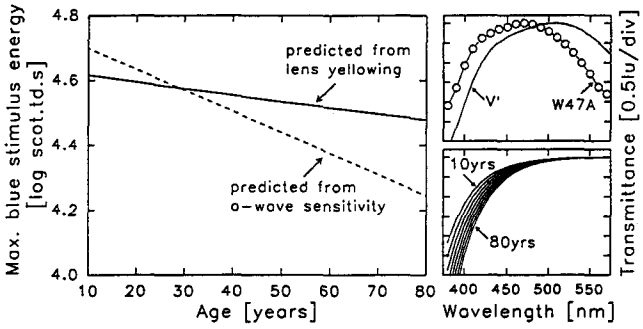

FIGURE 7. Left panel shows the estimated variation of retinal illuminance of the maximal blue stimulus with age of the subject. Dashed line is the prediction based on the measured age-related changes in rod-isolated *a*-wave sensitivity; solid line is the prediction based on an empirical model of lens yellowing. Top right panel is the spectral power distribution of the blue stimulus used (W47A) and the spectral luminous efficiency function (V'_λ) for scotopic vision. Bottom right panel is the average pre-retinal transmittance spectra based on an empirical model for subjects in the age range of 10–80 yr old.

parameters of the rod and cone photoreceptor versions of model 2 plotted as a function of age in a group of normal subjects. Rod fits were calculated by allowing R_{max} and σ_{sc} to vary in a six-wave ensemble (constants: τ_{sc} = 0.85 msec, δ = 1.1 msec, τ_{rm} = 0.5 msec). Cone fits were calculated similarly by allowing R_{max} and σ_{ph} to vary in a seven-wave ensemble (constants: τ_{ph} = 0.45 msec, δ = 1.1 msec, τ_{cm} = 2.0 msec). The regression lines for the rods had slopes of $-1.05\ \mu V\ yr^{-1}$ and -0.007 log scot $td^{-1}\ sec^{-3}\ yr^{-1}$, and *y*-intercepts of 500 μV and 1.80 log scot $td^{-1}\ sec^{-3}$ for R_{max} and σ_{sc}, respectively. The regression lines for cones had slopes of $-0.17\ \mu V\ yr^{-1}$ and 0.0005 log phot $td^{-1}\ sec^{-3}\ yr^{-1}$, and *y*-intercepts of 90 μV and 2.27 log phot $td^{-1}\ sec^{-3}$, for R_{max} and σ_{ph}, respectively. The correlation coefficients were 0.38 and 0.74 for rod R_{max} and σ_{sc}, respectively, and 0.40 and 0.06 for cone R_{max} and σ_{ph}, respectively. The rod sensitivity had a significant ($P < 0.005$) age component, declining approximately 0.1 log units per decade; the slopes of rod and cone maximum amplitudes and cone sensitivity were not significantly different from zero (Snedecor & Cochran, 1989).

It may be hypothesized that the age-related decline of sensitivity of the rod response is consistent with reduced retinal illumination due to the well known increase with age in pre-retinal absorption of shorter wavelength lights. To test this hypothesis, we estimated the expected reduction in retinal illumination of our blue stimulus. The estimate was based on an empirical model of lens yellowing (Savage *et al.*, 1993). Figure 7 (top right panel) shows the relative spectral power distribution of the blue stimulus (W47A) and the spectral luminous efficiency function (V'_λ) for scotopic vision (Wyszecki & Stiles, 1982). The curves are arbitrarily shifted vertically to equate their peak values. Figure 7 (bottom right panel) also shows the empirical pre-retinal absorption model for a range of ages between 10 and 80 yr (Savage *et al.*, 1993). For this work, the standard scotopic observer is assumed to be 30 yr old, and the incremental change with age in scotopic retinal illuminance of the blue stimulus is estimated.

Figure 7 (left panel) compares the age-related change in retinal illuminance due to lens yellowing (solid line) with the change predicted from the rod *a*-wave sensitivity data (dashed line). There appears to be a greater loss of *a*-wave sensitivity with age than that expected from pre-retinal absorption alone, thereby raising the possibility of a direct effect of age on the retina leading to change in the activation reactions of phototransduction.

DISCUSSION

In the present study, we demonstrate that an alternative simplification of the Lamb and Pugh (1992) model of phototransduction describes human ERG *a*-waves better than the currently used simplification, the delayed Gaussian. Our results show that the simplifying assumptions made during the derivation of the delayed Gaussian version prevent this model from being applied to responses evoked by high energy stimuli. In contrast, our alternative model fits the leading edge of both rod and cone *a*-wave families elicited by a range of stimuli from low energies to those causing significant bleaching (2.5% in rods, 1% in cones). Using the new model, we show that two waveforms are sufficient for the accurate estimation of phototransduction parameters, thus making shorter protocols and wider clinical application possible for the future. This study also satisfies an important prerequisite for clinical application by reporting normal rod and cone phototransduction parameters for a wide age range.

Rod phototransduction with high energy stimuli

The maximum rate of change per time (velocity) of the leading edge of human rod ERG *a*-wave has been shown to saturate with high stimulus energies (Breton & Montzka, 1992; Breton *et al.*, 1994). Our recordings are consistent with these previous observations. The saturation of the photocurrent velocity was originally reported in isolated rat retinas (Penn & Hagins, 1972) and further explored in isolated amphibian rods (Cobbs & Pugh, 1987). Penn and Hagins (1972) suggested that the observed velocity saturation is consistent with the effects of rod membrane capacitance. In isolated amphibian rods, Cobbs and Pugh (1987) showed experimentally that the rising phase of the bright flash response is dominated by cell membrane capacitance. Interestingly, however, photocurrent velocity saturation was observed even in voltage-clamped amphibian rods (Cobbs & Pugh, 1987). The underlying cause for velocity saturation of human ERG *a*-waves is not known, but our results with the alternative model can be used to support certain speculations.

Model 1 describes families of waveforms with a constant latency and an increasing rate of rise with higher stimulus energies. Therefore, it is not surprising that model 1 will not fit families of waveforms elicited by a range of stimulus energies as an ensemble [Fig. 5(a)]. Model 1 will however, describe such response families, if

the parameters are allowed to vary for each waveform [Fig. 5(b)]. Under these conditions, time delay and sensitivity parameters of model 1 appear to be dramatically reduced with higher stimulus energies [Fig. 5(e)].

We demonstrated that the alternative model (model 2) describes very well rod-isolated ERG *a*-wave families as an ensemble with a single set of parameters [Fig. 5(c)]. Therefore, our results suggest that the dramatic reduction of sensitivity and shortening of latency apparent when using model 1 may be an artefact of the breakdown of simplifying assumptions used. Considering the major difference between the two models is the explicit specification of the cascade of three first order impulse responses, we speculate that the observed saturation of the response velocity with high energy stimuli may be the result of increased prominence of the reaction delays at early times offsetting the increased rates of activation at higher energies. The smoothing effect of the membrane capacitance term of model 2 must also be playing a role in causing the saturation of response velocity, but simulations show this effect to be minor (see Appendix and Fig. A2).

Routine recording and modeling of photoreceptor function

With increasing prospects for treatment of photoreceptor diseases, means to monitor efficacy of therapy by measuring photoreceptor function directly and objectively are needed (Fulton & Breton, 1993). The recommended protocol for routine ERGs does not currently include bright flash recordings of rod- and cone-isolated *a*-waves but only a single white flash (*c.* 2.5 log scot td sec) in the dark-adapted state that elicits a mixed rod and cone response (Marmor *et al.*, 1989). At present, high energy rod-isolated ERG *a*-wave recordings require lengthy protocols and are mainly a research technique. If the phototransduction parameters could be reliably estimated from a small number of responses, the reduced testing time could allow the high energy ERG *a*-waves to be incorporated into a protocol that also includes the standardized ERG responses.

Our results suggest that only two rod-isolated responses, one evoked with high and one with low energy, are needed to reliably determine rod phototransduction parameters using model 2 and it should be feasible to incorporate these into a standardized ERG protocol. It is important to point out that in order to achieve rod-isolated responses at two energies using the double subtraction method, at least three blue (B1, B2, and B3) and two red (R1 and R2) responses are required. B1 would be the maximum stimulus energy limited by the stimulator available in the ERG clinic; R1 would be photopically matched to B1; B2 scotopically matched to R1; R2 photopically matched to B2; and, B3 scotopically matched to R2. In general, B3 will be of low enough energy that it is a pure rod response. For stimuli used in this work, the three blue stimulus energies would be: B1 = 4.6, B2 = 2.3, and B3 = 0.3 log scot td sec. B3 could be replaced by the rod response to a dim dark-adapted flash specified in the ERG standardized protocol (Marmor *et al.*, 1989), and the other four stimulus energies adjusted accordingly.

Cone phototransduction

In cones, like rods, a cGMP phosphodiesterase cascade is thought to mediate phototransduction (Haynes & Yau, 1985; Cobbs *et al.*, 1985). Although the specific molecular components of activation (e.g. Hurwitz *et al.*, 1985; Nathans *et al.*, 1986), the intrinsic gain, and the speed of the photocurrent are known to differ in the two types of receptors (Pugh & Cobbs, 1986), it may be hypothesized that the shape of the rising phase of the cone photocurrent is similar to that of the rod photocurrent. This hypothesis finds support from the recent reanalysis of previously published data showing that model 1 fits photocurrents recorded from single cone photoreceptor cells (Pugh & Lamb, 1993).

The relationship between corneally recorded cone-isolated ERG *a*-waves and underlying cone receptor photocurrents is not as well established as for rods and is still being investigated. For example, it was recently observed that only waveforms to high energies and at short times post-stimulus directly relate to the sum of cone receptor photocurrents; the negativity at lower energies has a major post-receptoral contribution (Sieving *et al.*, 1994; Bush & Sieving, 1994). Also, the computational models fitted to rods and cones differ; specifically, rods appear to saturate as an exponential whereas cones as a Michaelis–Menten function of stimulus energy (Hood & Birch, 1993b; Bush & Sieving, 1994). However, taking into consideration the extensive outer segment membrane area of the cone, and the addition of a single low-pass filter stage to model 1, good fits to cone *a*-wave data have been achieved (Hood & Birch, 1993b, 1995). The model derived in this paper, which already includes a membrane capacitance term, fitted the leading edge of cone *a*-waves very well.

Amplification in rod and cone transduction

The amplification [parameter A in Equation (20); Pugh & Lamb (1993)] of the photon signal in individual photoreceptors has been defined. Using ERG *a*-waves, the amplification in human rod and cone photoreceptors may be estimated if the number of isomerizations caused per troland is available. Recent estimates for these parameters are nine isomerizations per rod per scot td (Breton *et al.*, 1994), and 13 isomerizations per L-cone per phot td (Hood & Birch, 1995). Using the alternative model and mean normal values for σ_{sc} and σ_{ph}, the estimated amplification factors for normals are 3.7 and 15 sec^{-2}, for rods and cones, respectively. These results are similar to other estimates based on model 1 (Pugh & Lamb, 1993; Breton *et al.*, 1994; Hood & Birch, 1995). It has been hypothesized that mammalian rods and cones do not differ greatly in amplification (Pugh & Lamb, 1993). The apparent four-fold difference in amplification between rods and cones in the present study does not currently warrant rejection of the hypothesis that they are

similar, because of the relatively large uncertainty associated with relating stimulus energy measured at the cornea with the number of isomerizations at the retina.

Delay of rod and cone activation

Model 1 lumps all biochemical and technical delays together whereas model 2 explicitly and quantitatively separates them into three types; delays caused by the stimulation and recording system (δ), the delays of activation reactions (τ_{sc} for rods and τ_{ph} for cones) and the delays due to the capacitance of the photoreceptor membrane (τ_{rm} for rods and τ_{cm} for cones). This study showed that the time constant of activation for cones (τ_{ph} = 0.45 msec) is approximately half as large as the that for the rods (τ_{sc} = 0.85 msec). Assuming a cascade of three first-order reactions with equal time constants dominate the activation of the phototransduction cascade in both receptor types, our results suggest that reactions in human cone photoreceptors must proceed much faster than those in rods. Alternatively, there may be less than three reactions with dominant time constants in cone activation. Our results are in general agreement with those of Hood and Birch (1993b, 1994, 1995), who reported a time delay for the cones (using a modified version of model 1) that is shorter than the time delay for the rods (using model 1). Furthermore, our results appear also to be in agreement with time delays recorded under voltage clamp from single rod and cone photoreceptors (Pugh & Lamb, 1993).

It was somewhat surprising that the *a*-waves of all normal subjects were very well fit by rod and cone time constants of activation that were held invariant. It is not known at this time whether data from patients with retinal disease will be equally well fit by the same normal values of rod and cone time constants. In this regard, it is interesting that there have not been any reports to date of patients showing abnormalities in time delay (Cideciyan & Jacobson, 1993; Breton *et al.*, 1994; Jacobson *et al.*, 1994; Hood & Birch, 1994, 1995; Hood *et al.*, 1995). As we have shown in Fig. 2, there is a trade-off between time delay and sensitivity when using model 1. Thus, small abnormalities in time delay may not be detectable unless *a*-wave responses evoked by high energy stimuli are characterized using an appropriate model of phototransduction.

Aging and phototransduction

The age-related variation in standard ERG parameters has been described (Weleber, 1981; Aylward *et al.*, 1990; Birch & Anderson, 1992) but the variations in rod- and cone-isolated ERG *a*-wave phototransduction parameters are not established. In two short reports on the topic, different conclusions are reached on the effects of age on rod-isolated ERG *a*-waves. In one study, there was an age-related decline of sensitivity but not of maximum amplitude (Birch & Hood, 1993). In another study, there was no age-related decline of sensitivity but a decline of maximum amplitude (Breton & Patel, 1995). There are no reports of the relation between high energy cone-isolated *a*-waves and age. The data in the present study are consistent with Birch and Hood (1993) in showing an age-related decline of rod sensitivity, but no significant age-related decline in rod maximum amplitude. Additionally, we found no significant age-related changes in cone sensitivity and maximum amplitude.

Two of the most obvious nonretinal causes that may result in an apparent reduction of response sensitivity are age-related reduction of maximal pupil diameter and age-related lens yellowing. Pupil diameter changes would be expected to result in equal reduction in rod and cone *a*-wave sensitivity, whereas lens yellowing would predominantly affect the rod results due to the use of the short wavelength stimulus. Our results show an age-related decline in rod sensitivity but not in cone sensitivity.

Using a model of lens yellowing, we showed that the loss of rod *a*-wave sensitivity is much larger than that expected from pre-retinal absorption. Further studies with greater numbers of subjects and subject-specific estimates of pre-retinal absorption are required in order to confirm this finding. Within the limitations of sample size and an empirical pre-retinal absorption model, our results prompt the speculation that age-related changes in the transduction machinery may exist. One possible explanation for the decrease in rod sensitivity is that age-related accumulation of cholesterol may decrease the fluidity of disc membranes and thus decrease the rate of PDE activation (Boesze-Battaglia & Albert, 1990; Eldred, 1993).

The maximum amplitude parameters of the rod and cone ERG *a*-waves are believed to represent the outer segment membrane area (Breton *et al.*, 1994; Hood & Birch, 1996). Reduction of the maximum amplitude in retinal disease has been suggestive of photoreceptor dropout and/or outer segment shortening (Cideciyan & Jacobson, 1993; Jacobson *et al.*, 1994; Hood & Birch, 1994; Breton *et al.*, 1994). Our finding of no significant age-related change in rod and cone maximum amplitudes would suggest that the average outer segment membrane area per unit retinal area in the peripheral field is not significantly changing with age. It is of interest to try to relate our findings to morphologically determined rod and cone cell densities. If we assume that:

1. Peripheral photoreceptors mainly contribute to the full-field ERG;
2. All peripheral photoreceptor outer segments have similar lengths and diameters that do not change with age; and
3. There are no age-related changes in the size or resistive pathways of the eye,

then *a*-wave maximum amplitude would be expected to relate directly to spatial density of peripheral photoreceptors.

Using human donor eyes, Gao and Hollyfield (1992) found small age-related reductions in the peripheral rod (−4.6% per decade) and cone (−3.3% per decade) cell

densities, whereas Curcio *et al.* (1993) found no significant age-related change in peripheral rod cell density (−2.8% per decade) and a small age-related reduction in peripheral cone cell density (−3.1% per decade). Our regression analysis showed small, but not significant, reductions for rod (−2.2% per decade) and cone (−2.0% per decade) maximum amplitude parameters. Considering the extent of the assumptions needed to compare the physiology and the morphology, our *a*-wave results are generally consistent with the relatively small age-related changes seen histologically.

REFERENCES

Aylward, G. W., Jeffrey, B. G. & Billson, F. A. (1990). Normal variation and the effect of age on the parametric analysis of the intensity-response series of the scotopic electroretinogram, including the scotopic threshold response. *Clinical Vision Sciences, 5*, 353–362.

Baylor, D. A., Nunn, B. J. & Schnapf, J. L. (1984). The photocurrent, noise, and spectral sensitivity of rods of the monkey *Macaca fascicularis*. *Journal of Physiology, 357*, 575–607.

Birch, D. G. & Anderson, J. L. (1992). Standardized full-field electroretinography. Normal values and their variation with age. *Archives of Ophthalmology, 110*, 1571–1576.

Birch, D. G. & Hood, D. C. (1993). Inner and outer retinal contributions to age changes in rod ERGs from normal subjects. *Investigative Ophthalmology and Visual Science, ARVO Abstracts, 34*, 1079.

Boesze-Battaglia, K. & Albert, A. D. (1990). Cholesterol modulation of photoreceptor function in bovine retinal rod outer segments. *Journal of Biological Chemistry, 265*, 20727–20730.

Breton, M. E. & Montzka, D. P. (1992). Empiric limits of rod photocurrent component underlying *a*-wave response in the electroretinogram. *Documenta Ophthalmologica, 79*, 337–361.

Breton, M. E. & Patel, M. B. (1995). Age related change in ERG a-wave and b-wave amplitudes and amplification constant of phototransduction. *Investigative Ophthalmology and Visual Science, 36*, S924.

Breton, M. E., Schueller, A. W., Lamb, T. D. & Pugh, E. N. Jr. (1994). Analysis of ERG a-wave amplification and kinetics in terms of the G-protein cascade of phototransduction. *Investigative Ophthalmology and Visual Science, 35*, 295–309.

Bush, R. A. & Sieving, P. A. (1994). A proximal retinal component in the primate photopic ERG a-wave. *Investigative Ophthalmology and Visual Science, 35*, 635–645.

Cideciyan, A. V. & Jacobson, S. G. (1993). Negative electroretinograms in retinitis pigmentosa. *Investigative Ophthalmology and Visual Science, 34*, 3253–3263.

Cobbs, W. H., Barkdoll, A. E. III & Pugh, E. N. Jr. (1985). Cyclic GMP increases photocurrent and light sensitivity of retinal cones. *Nature, 317*, 64–66.

Cobbs, W. H. & Pugh E. N. Jr. (1987). Kinetics and components of the flash photocurrent of isolated retinal rods of the larval salamander, *Ambystoma tigrinum*. *Journal of Physiology, 394*, 529–572.

Curcio, C. A., Millican, C. L., Allen, K. A. & Kalina, R. E. (1993). Aging of the human photoreceptor mosaic: Evidence for selective vulnerability of rods in central retina. *Investigative Ophthalmology and Visual Science, 34*, 3278–3296.

Eldred, G. E. (1993). Biochemical aging in the retina and RPE. In Osborne, N. & Chader, G. (Eds), *Progress in retinal research* (pp. 101–131). Oxford: Pergamon Press..

Findl, O., Hansen, R. M. & Fulton, A. B. (1995). The effects of acetazolamide on the electroretinographic responses in rats. *Investigative Ophthalmology and Visual Science, 36*, 1019–1026.

Fulton, A. B. & Breton, M. E. (1993). Clinical physiology of heritable photoreceptor diseases. *Archives of Ophthalmology, 111*, 1479–1481.

Gao, H. & Hollyfield, J. G. (1992). Aging of the human retina: Differential loss of neurons and retinal pigment epithelial cells. *Investigative Ophthalmology and Visual Science, 33*, 1–17.

Granit, R. (1933). The components of the retinal action potential in mammals and their relation to the discharge in the optic nerve. *Journal of Physiology, 77*, 207–239.

Haynes, L. W. & Yau, K.-W. (1985). Cyclic GMP-sensitive conductance in outer segment membranes of catfish cones. *Nature, 317*, 61–64.

Hood, D. C. & Birch, D. G. (1990). A quantitative measure of the electrical activity of human rod photoreceptors using electroretinography. *Visual Neuroscience, 5*, 379–387.

Hood, D. C. & Birch, D. G. (1993a). Light adaptation of human rod receptors: The leading edge of the human *a*-wave and models of rod receptor activity. *Vision Research, 33*, 1605–1618.

Hood, D. C. & Birch, D. G. (1993b). Human cone receptor activity: The leading edge of the *a*-wave and models of receptor activity. *Visual Neuroscience, 10*, 857–871.

Hood, D. C. & Birch, D. G. (1994). Rod phototransduction in retinitis pigmentosa: Estimation and interpretation of parameters derived from the rod a-wave. *Investigative Ophthalmology and Visual Science, 35*, 2948–2961.

Hood, D. C. & Birch, D. G. (1995). Phototransduction in human cones measured using the a-wave of the ERG. *Vision Research, 35*, 2801–2819.

Hood, D. C. & Birch, D. G. (1996). Abnormalities of the retinal cone system in retinitis pigmentosa. *Vision Research, 36*, 1699–1709.

Hood, D. C., Cideciyan, A. V., Roman, A. J. & Jacobson, S. G. (1995). Enhanced S cone syndrome: Evidence for an abnormally large number of S cones. *Vision Research, 35*, 1473–1481.

Hurwitz, R. L., Bunt-Milam, A. H., Chang, M. L. & Beavo, J. A. (1985). cGMP phosphodiesterase in rod and cone outer segments of the retina. *Journal of Biological Chemistry, 260*, 568–573.

Jacobson, S. G., Kemp, C. M., Cideciyan, A. V., Macke, J. P., Sung, C.-H. & Nathans, J. (1994). Phenotypes of stop codon and splice site rhodopsin mutations causing retinitis pigmentosa. *Investigative Ophthalmology and Visual Science, 35*, 2521–2534.

Lamb, T. D. (1994). Stochastic simulation of activation in the G-protein cascade of phototransduction. *Biophysical Journal, 67*, 1439–1454.

Lamb, T. D. & Pugh, E. N. Jr. (1992). A quantitative account of the activation steps involved in phototransduction in amphibian photoreceptors. *Journal of Physiology, 449*, 719–758.

Marmor, M. F., Arden, G. B., Nilsson, S. E. G. & Zrenner, E. (1989). Standard for clinical electroretinography. *Archives of Ophthalmology, 107*, 816–819.

Nathans, J., Thomas, D. & Hogness, D. S. (1986). Molecular genetics of human color vision: The genes encoding blue, green and red pigments. *Science, 232*, 193–202.

Nelder, J. A. & Mead, R. (1965). A simplex method for function minimization. *Computer Journal, 7*, 308–313.

Palczewski, K. (1994). Is vertebrate phototransduction solved? New insights into the molecular mechanism of phototransduction. *Investigative Ophthalmology and Visual Science, 35*, 3577–3581.

Penn, R. D. & Hagins, W. A. (1969). Signal transmission along retinal rods and the origin of the electroretinographic *a*-wave. *Nature, 223*, 201–205.

Penn, R. D. & Hagins, W. A. (1972). Kinetics of the photocurrent of retinal rods. *Biophysical Journal, 12*, 1073–1096.

Pugh, E. N. Jr & Cobbs, W. H. (1986). Visual transduction in vertebrate rods and cones: A tale of two transmitters, calcium and cyclic GMP. *Vision Research, 26*, 1613–1643.

Pugh, E. N. Jr & Lamb, T. D. (1993). Amplification and kinetics of the activation steps in phototransduction. *Biochimica et Biophysica Acta, 1141*, 111–149.

Sandberg, M. A., Miller, S. & Berson, E. L. (1990). Rod electroretinograms in an elevated cyclic guanosine monophosphate-type human retinal degeneration. *Investigative Ophthalmology and Visual Science, 31*, 2283–2287.

Savage, G. L., Haegerstrom-Portnoy, G. & Adams, A. J. (1993). Age changes in the optical density of human ocular media. *Clinical Vision Sciences, 8*, 97–108.

Sieving, P. A., Murayama, K. & Naarendorp, F. (1994). Push–pull model of the primate photopic electroretinogram: A role for hyperpolarizing neurons in shaping the *b*-wave. *Visual Neuroscience, 11*, 519–532.

Snedecor, G. W. & Cochran, W. G. (1989). *Statistical methods* (8th Ed, pp. 186–187). Iowa: Iowa State University Press, AMES..

Weleber, R. G. (1981). The effect of age on human cone and rod ganzfeld electroretinograms. *Investigative Ophthalmology and Visual Science, 22*, 392–399.

Wyszecki, G. & Stiles, W. S. (1982). *Color science* (2nd Ed., pp. 107–112 and pp. 256–259). New York: John Wiley & Sons.

Acknowledgements—Supported in part by Public Health Service Research Grant EY05627, The Foundation Fighting Blindness (Baltimore, MA/(Rosslyn, VA)) and The Whitaker Foundation. The authors thank Drs Trevor D. Lamb, Donald C. Hood, Edward N. Pugh, Jr and Colin M. Kemp for insightful and constructive comments; and Mr William J. Feuer for statistical consultation.

APPENDIX

Derivation of the Alternative Model of Phototransduction

The accepted theory of phototransduction in the rod photoreceptor relates the absorption of a photon by a rhodopsin molecule embedded in a disc membrane to the closing of cation channels embedded in the plasma membrane (Palczewski, 1994). The biochemical reactions occurring at the disc membrane include the activations of rhodopsin ($Rh \rightarrow Rh^*$), of G-protein ($G \rightarrow G^*$), and of phosphodiesterase ($PDE \rightarrow PDE^*$). The quantitative description of these reactions is summarized by [Equation (3.1); Lamb & Pugh (1992)];

$$PDE^*(t) = \Phi \cdot \nu_{RP} \cdot \text{ramp}(t) \star \text{delay}(\tau_R, \tau_{2C}, \tau_{2E}, \tau_{P1}, \tau_{P2}, \tau_{P3}, t) \tag{A1}$$

where $PDE^*(t)$ is the number of activated PDE subunits at time t; Φ, the number of isomerizations caused by an impulsive flash of light at time zero; ν_{RP}, the number of PDE^* produced by each Rh^*; ramp(), short-hand for $y = 0$ for $t < 0$ and $y = t$ for $t \geq 0$; $\star$, short-hand for convolution; and delay(), short-hand for the impulse response of several cascaded first order delay stages. There are six delay stages considered in Equation (A1) with the following time constants; τ_R for activation of Rh, τ_{2C} for binding of GTP to G-protein, τ_{2E} for the separation of the GTP bound G-protein into its subunits, τ_{P1} for first contact between G^* and a PDE, τ_{P2} for the reaction of G^* with PDE, and τ_{P3} for the removal of inhibition of the PDE.

When the individual delay stages shown in Equation (A1) are small with respect to the time scale of the response of interest, Equation (A1) can be approximated by a delayed and scaled ramp [Equation (3.3); Lamb & Pugh (1992)]:

$$PDE^*(t) \approx \Phi \cdot \nu_{RP} \cdot \text{ramp}(t - t_{\text{eff}}) \tag{A2}$$

where t_{eff} is a short time delay.

Photoreceptor dark current flows due to cytoplasmic cGMP holding open the cation channels in the plasma membrane. The light-evoked blockage of this dark current is quantified based on the hydrolysis of the cytoplasmic cGMP by PDE^* [Equation (6.6); Lamb & Pugh (1992)]:

$$R(t) = 1 - exp\left(-\Phi\left[n \cdot \beta_{\text{sub}} \cdot \int_0^t PDE^*_\Phi(t')\,dt'\right]\right) \tag{A3}$$

where $R(t)$ is the normalized photocurrent at time t; n, the co-operativity index of the cation channel; β_{sub}, the hydrolytic rate constant per PDE^*; and $PDE^*_\Phi(t) = PDE^*(t)/\Phi$.

Substituting Equation (A2) into Equation (A3), the "delayed Gaussian" approximation of phototransduction is derived [Equation (6.10); Lamb & Pugh (1992)]:

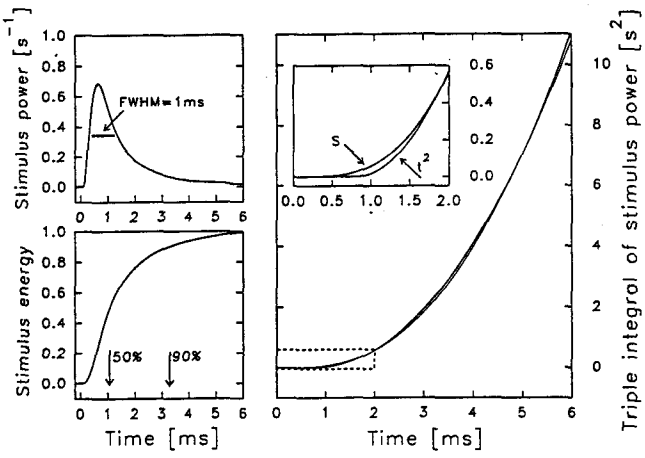

FIGURE A1. Top left panel is the radiant flux of the stimulus flash used in this work; the function is normalized to have a unit integral. Full-width-at-half-maximum is shown. Bottom left panel is the cumulative energy of the stimulus calculated by numerical integration of the radiant flux curve shown above. The 50 and 90% cumulative energy time points are shown with arrows. Right panel is the triple time integral of the stimulus radiant flux (S) compared to a delayed quadratic (t^2). The area enclosed by dashed lines is shown enlarged in the inset.

$$R(t) = 1 - exp\left\{-\frac{1}{2}\Phi\left[\frac{t - t_{\text{eff}}}{\tau_\phi}\right]^2\right\}, \quad t > t_{\text{eff}} \tag{A4}$$

where τ_Φ is the so-called "characteristic time constant of transduction". Note that model 1 defined in Equation (1) in the text is of the same form as Equation (A4).

To summarize briefly there are three integrating steps in the phototransduction cascade theory (Pugh & Lamb, 1993):

1. The production of Rh^* by the stimulus;
2. Activation of many G-proteins by each Rh^*; and
3. Drop of cytoplasmic cGMP concentration due to the increased number of PDE^*.

The integrating steps (1) and (2) are implicitly shown in Equation (A1) where the ramp() function is the double integral of the stimulus function which is assumed to be an impulse. The integrating step (3) is shown explicitly in Equation (A3); the t^2 term in Equation (A4) is due to triple integration of the impulsive stimulus.

Equation (A4) was derived based on many assumptions and approximations that have been detailed (Lamb & Pugh, 1992; Pugh & Lamb, 1993). Here we concentrate on the following three assumptions:

1. The stimulus is an impulse causing all isomerizations to occur at time zero;
2. The time scale of the response is much slower than the effective time delay; and
3. The photocurrent is being measured directly from a photoreceptor outer segment.

None of these assumptions are valid for human ERG *a*-waves recorded with high energy stimuli.

An alternative model can be derived that uses the same quantitation of the activation reactions of phototransduction but does not make the restrictive assumptions listed above. First we rewrite the activation phase of the phototransduction for a nonimpulsive stimulus and explicitly show the three integrating steps;

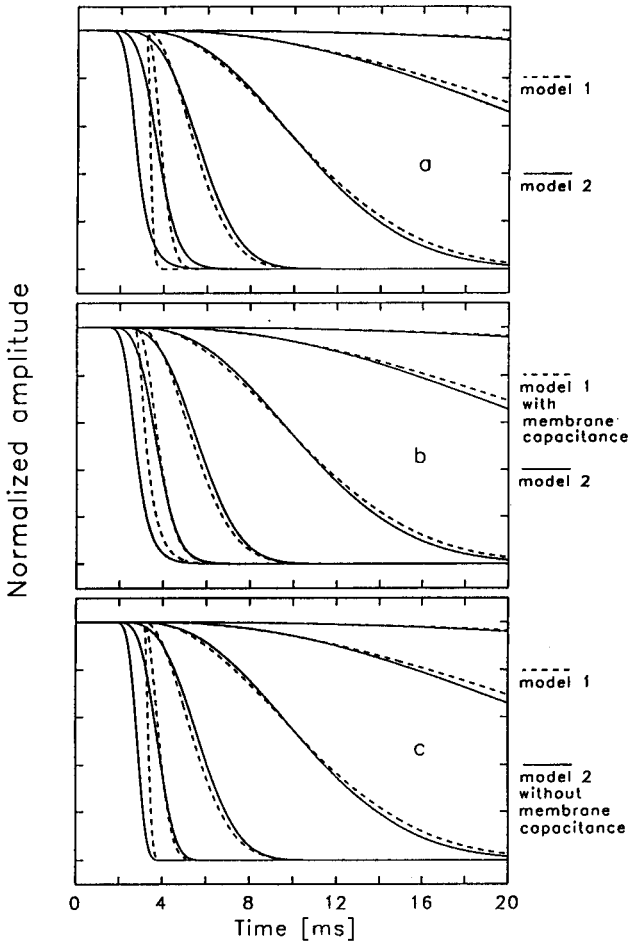

FIGURE A2. The effect of the membrane capacitance term on model 1 (dashed lines) and model 2 (solid lines). The stimulus energies are chosen from 1 to 6 log scot td sec in 1 log unit steps; faster responses correspond to higher energies. (a) Comparison of the two models using respective mean normal parameter values. (b) Comparison of model 2 with modified model 1 which includes a convolution with a 0.5 msec time constant membrane capacitance term and reduction of the t_{eff} by 0.5 msec to compensate for the convolution. (c) Comparison of model 1 with modified model 2 which includes removal of the convolution with the membrane capacitance term and increase of δ by 0.5 msec to compensate.

$$I(\Phi,t) = 1 - exp\left(-k\Phi\left\{\int_0^t\int_0^{t'''}\int_0^{t''}\lambda_\Phi(t')dt'dt''dt'''\right\} \star \text{delay}(\tau_1,\tau_2,...,\tau_m,t)\right) \quad \text{(A5)}$$

where $I(\Phi,t)$ is the normalized photocurrent; Φ, the total number of isomerizations caused by the light stimulus; t, the time in seconds; k, a constant in sec^{-2}; $\lambda_\Phi(t)$, the stimulus function in sec^{-1}, normalized by the total number of isomerizations so that it has a unit integral with respect to time; t', t'', t dummy variables of integration representing time; delay(), impulse response of a cascade of first-order delay stages in the activation phase of the phototransduction; and $\star$, the convolution operation.

Figure A1 (top left) shows the normalized stimulus function, $\lambda_\Phi(t)$, recorded with an 8 kHz bandwidth and sampled at 20 kHz. It has a full-width-at-half-maximum duration of 1 msec. Figure A1 (bottom left) displays the cumulative energy (first integral; calculated numerically) of the stimulus function; 50% cumulative energy is at 1 msec and 90% at *c.* 3 msec. It may be noted that the triple integration of $\lambda_\Phi(t)$ with respect to time produces a function that has units of sec^2. More specifically, this triple integral [term in curly brackets, Equation (A5)], can be well approximated by a simple quadratic

$$\left\{\int_0^t\int_0^{t'''}\int_0^{t''}\lambda_\Phi(t')dt'dt''dt'''\right\} \approx \frac{1}{2}(t-\delta)^2, \quad t \geq \delta \quad \text{(A6)}$$

where δ is a short time delay in seconds. The comparison of the triple integral (calculated numerically) of the normalized stimulus function with a delayed quadratic is shown in Fig. A1 (right panel). The best fit value of δ is 0.8 msec. It is important to note that when the stimulus function is an impulse, its triple integral is $\frac{1}{2}t^2$ [see Equation (A4)]. Thus, we are approximating the effects of the triple integral of a nonimpulsive stimulus with the triple integral of an impulsive stimulus delayed in time.

Substituting Equation (A6) into Equation (A5) is a preliminary step towards mathematical tractability. With the aim of further simplification, it is noted that the delay() term originates from several cascaded activation reactions, assumed to be first-order and occurring during the earliest stages of phototransduction. Currently available biochemical data suggest that three of these cascades of reactions in rod receptors have dominant time constants:

1. Formation of Rh^*;
2. The activation of the G-protein by an Rh^*; and
3. The activation of the PDE.

In mammalian photoreceptors at 37°C, Rh^* formation [τ_R in Equation (A1)] is estimated to be *c.* 0.5 msec (Pugh & Lamb, 1993). The activation of G-protein is hypothesized to involve five microsteps (Pugh & Lamb, 1993). The first four microsteps should not take longer than 0.1 msec (Pugh & Lamb, 1993). The kinetics of the fifth microstep [τ_{2E} in Equation (A1)], dissociation of G·GTP into G_α·GTP and $G_{\beta\gamma}$, is currently not known and it may involve a larger delay (Pugh & Lamb, 1993). For the activation of PDE, it is believed that the first contact time [τ_{P1} in Equation (A1)] is the dominant time constant and it is estimated to be longer than 0.2 msec (Pugh & Lamb, 1993). Because these three reactions appear to have time constants in the neighborhood of 0.1–1.0 msec, it is possible to simplify the delay() term into a cascade of three first-order reactions, each with the *same* time constant. The impulse response is:

$$\text{delay}(\tau_1,\tau_2,\tau_3,t) \approx \text{delay}(\tau,\tau,\tau,t) = \frac{t^2}{2\tau^3}exp\left(\frac{t}{\tau}\right) \quad \text{(A7)}$$

where τ is the time constant of the three decays presumed to be dominant stages of rod activation. Substituting Equations (A7) and (A6) into Equation (A5), and performing the convolution, the following result is derived:

$$I(\Phi,t) = 1 - exp\left(-\frac{1}{2}k\cdot\Phi\left\{(\epsilon^2 - 6\epsilon\tau + 12\tau^2) - e^{-\frac{\epsilon}{\tau}}(\epsilon^2 + 6\epsilon\tau + 12\tau^2)\right\}\right) \quad \text{(A8)}$$

where $\epsilon = t - \delta$; is the delayed time. It is important to note that the delay, δ, is not an additional parameter; it is a recording-system-specific constant and does not vary with the subject tested. Furthermore, there may be other system-specific pure time delays that may be incorporated into δ. Such a significant time delay is introduced, for example, by the amplifier. The frequency response of the amplifier used in this work was determined to have a flat gain, and an approximately linear phase shift corresponding to a constant time delay of 0.3 msec, in the 50–500 Hz range (data not shown). Delays introduced by other components of the recording system are estimated to be much less than 0.1 msec. Therefore, for the system used in this work δ is set equal to 1.1 msec (0.8 msec due to flash and 0.3 msec due to amplifier).

The normalized photocurrent defined by Equation (A8) may be recordable with single cell techniques in voltage-clamped conditions that eliminate the capacitive current, but this is not feasible in noninvasive ERG *a*-wave recordings. Instead, the sum of the field

potentials created by the photocurrrent is being measured. Thus the low-pass filtering effect of the membrane capacitance needs to be included for the model to be useful. This can be achieved by convolving Equation (A8) with a truncated exponential. The resulting equation for the potential measured at the cornea is shown as Equation (2) in the main body of this paper. The approximate capacitive time constants of rod (τ_{rm}) and cone (τ_{cm}) photoreceptor membranes are difficult to estimate. Values of 1 msec for rat rods (Penn & Hagins, 1972) and 1.8 msec for human cones (Hood & Birch, 1995, 1996) have been suggested. In this work, time constants of 0.5 msec for rods and 2.0 msec for cones were used.

As we show in the main body of this paper, families of *a*-waves evoked by high energy stimuli are described with our alternative model better than with the delayed Gaussian model. The question may arise whether the addition of a capacitive filtering term to the delayed Gaussian model is all that is needed. Figure 9 demonstrates that the filtering stage with the capacitive time constant is important but it is not the major difference between the models. Figure A2(a) shows the two models with their respective mean normal parameters. Figure A2(b) shows the effect of adding a capacitive filtering stage to model 1; Fig. A2(c) shows the effect of removing the capacitive filtering stage from model 2. In all three panels of Fig. A2, the two models are very similar up to 4 log scot td sec; differences are apparent mostly at the two highest energy responses. Figure A2(b) shows that the capacitance term reduces the velocity of the high energy responses predicted by model 1. This moves model 1 more toward the behavior of ERG *a*-waves but significant differences still remain due to fixed latency. Figure A2(c) shows that the effect of the capacitance term in the alternative model can be described as a simple delay up to *c.* 5 log scot td sec; at higher energies, the waveform velocity is significantly reduced due to capacitance. Therefore, we can conclude that the major difference between the two models is that the alternative model explicitly specifies the impulse response of three cascaded first order decays, whereas the delayed Gaussian model approximates them with a pure time delay.